

Particle density and critical point for studying site percolation by finite size scaling

Dian Xu,¹ Shanshan Wang,¹ Feng Gao,¹ Wei Li,^{1,*} and Jianmin Shen^{1,2,†}

¹*Key Laboratory of Quark and Lepton Physics (MOE) and Institute of Particle Physics, Central China Normal University, Wuhan 430079, China*

²*School of engineering and technology, Baoshan University, Baoshan 678000, China*

(Dated: May 9, 2024)

Machine learning has recently achieved remarkable success in studying phase transitions. It is generally believed that the latent variables of unsupervised learning can capture the information related to phase transitions, which is usually achieved through the so-called order parameter. In most models, for instance the Ising, the order parameters are simply the particle number densities. The percolation, the simplest model which can generate a phase transition, however, has a unique order parameter which is not particle number density. In this paper, we use unsupervised learning to study the relationship between particle number density, critical point, and latent variables in the site percolation model. It is found that if the input of learning is the original configuration, then the output of unsupervised learning does not convey any information related to the phase transition. Therefore, the maximum cluster is employed in order to effectively capture the critical point of the model. Unsupervised learning yields reliable results consistent with Monte Carlo simulations. We also propose a method called Fake Finite Size Scaling (FFSS) to calculate the critical value, which improves the accuracy of fitting to a great extent.

I. INTRODUCTION

Machine Learning (ML) [1, 2] is a specialized area of artificial intelligence (AI) that focuses on creating algorithms [3] and statistical models [4]. These models enable computers to perform tasks without explicit instructions [5]. ML allows computers to learn from data [6], enabling them to make decisions, predictions, or identify patterns independently [7, 8]. This capability is particularly valuable for data analysis in the field of physics. It offers an alternative approach, alongside theoretical calculations [9], numerical simulations [10, 11], and field theory [12], for analyzing phase transitions in statistical physics.

The integration of ML techniques into the investigation of phase transitions constitutes a fascinating amalgamation of condensed matter physics, computational science, and data-driven methodologies [13–16]. While computational methods, exemplified by Monte Carlo (MC) simulations [9], have been deployed for studying phase transitions for many years, the application of ML techniques represents a more recent advancement. Initially, in the nascent stages of computationally studying phase transitions, the primary emphasis was placed on the utilization of traditional computational physics techniques such as MC simulations, molecular dynam-

ics [17–19], and density functional theory [20, 21]. These methodologies primarily entailed deterministic or statistical approaches. However, with the emergence of vast datasets and improved computing capabilities, scientists began to explore the potential of employing data-driven approaches in this field [22, 23]. In the late 2000s and early 2010s, preliminary investigations were undertaken to employ techniques such as pattern recognition [21] to detect and characterize phases and phase transitions in complex systems [24]. An early milestone in this domain involved the utilization of supervised learning algorithms, including Support Vector Machines [25–27], to detect critical points during phase transitions, showcasing superior accuracy compared to traditional methods. Furthermore, ML, particularly techniques like Principal Component Analysis (PCA) [28], has demonstrated efficacy in identifying the key factors influencing phase transitions, thereby simplifying complex challenges in this area. Subsequently, in the mid-2010s, researchers commenced the adoption of unsupervised learning techniques [29, 30], encompassing clustering and neural network-based generative models, to unveil previously unknown phases or propose new modalities of phase transitions. Notably, ML techniques, especially neural networks tailored for handling quantum states, have rendered quantum phase transitions more amenable to study, despite their intrinsic challenges.

ML possesses the potential to mitigate various

* liw@mail.ccnu.edu.cn

† sjm@mails.ccnu.edu.cn

challenges inherent in percolation models, furnishing invaluable insights that prove elusive through conventional computational or analytical methodologies. Percolation theory entails the determination of the percolation threshold [31, 32], a pivotal juncture marking the system’s transition from a non-percolated to a percolated state. ML stands poised to facilitate the precise and expeditious identification of this threshold. Percolation models frequently encompass parameters such as porosity, viscosity, and temperature [33]. Through the employment of ML algorithms, we can elucidate the relative significance of these attributes in shaping percolation phenomena. By leveraging ML techniques such as clustering, we can scrutinize the distribution and attributes of percolated clusters, thereby gaining insights into the microscopic intricacies of percolation [34]. Furthermore, ML holds the capability to optimize the design of experiments or simulations aimed at exploring the parameter space with greater efficiency, culminating in swifter and more accurate comprehension of percolation dynamics [35, 36].

Numerous investigations have underscored the efficacy of unsupervised learning in capturing the order parameter information of phase transition systems [13, 16, 20, 37–40]. Nevertheless, it’s worth noting that the order parameter of the site percolation model transcends a mere particle number density, encompassing instead the probability that a lattice site pertains to a percolating cluster. Motivated by this insight, the present study will employ MC methods to compute the particle number density of the site percolation model, complemented by the utilization of unsupervised learning techniques to reduce model dimensionality. Both endeavors converge towards a common objective: the determination of the critical point, pivotal for investigating the interplay between particle number density and criticality. The principal methodology entails the shuffling or selection of maximum clusters, subsequently inputted into the algorithm to discern alterations in the output.

The primary structure of this paper unfolds as follows. Section II A elucidates the phase transition models of interest. Section II B expounds upon the two methodologies of PCA and Autoencoders (AE). Section III delineates the research findings, wherein a comparative analysis of four distinct configurations under MC, PCA, and AE is presented. Finally, in Section IV, we furnish a comprehensive summary of this study.

II. MODEL AND METHODS

A. The Percolation model

In the site percolation model [41, 42], we adopt a regular lattice as the foundational structure. A lattice, resembling a grid-like arrangement, assigns each point one of two states: "occupied" or "empty". The occupation of a site transpires with a probability p , irrespective of the states of neighboring sites. Each square within the lattice can manifest either as empty or occupied. The likelihood of a square being occupied is denoted by p , while the likelihood of it being empty is represented by $1 - p$. Crucially, the focal point lies in discerning the existence of a contiguous cluster of occupied squares spanning from one end of the lattice to the other.

To probe the site percolation model [43, 44], the ensuing steps may be undertaken: Firstly, initialization of the lattice: Commence by constructing a lattice comprising $N \times N$ sites, particularly in the context of a two-dimensional square lattice. Secondly, random occupation: Progress to randomly populate each site with a specified probability, designated as p . Thirdly, identification of clusters: Assign labels to the connected clusters of occupied sites. Two occupied sites are deemed part of the same cluster if they are contiguous to each other. Fourthly, percolation assessment: Scrutinize whether any of the clusters traverse the lattice from one end to the other, signifying percolation. Finally, iterate for robust statistical insights: To procure reliable statistics, iterate through the aforementioned steps multiple times.

In the scenario of a square lattice, a critical probability denoted as p_c emerges, commonly referred to as the percolation threshold. When the probability remains below p_c , the occurrence of a spanning cluster within the system is highly improbable. Conversely, as the probability surpasses p_c , the probability of encountering a percolating cluster swiftly converges to unity with increasing lattice dimensions.

Typically, the phenomenon of percolation manifests predominantly within the largest cluster [45]. Consequently, this article abstains from considering secondary or smaller clusters. For two-dimensional site percolation, the critical value is $p_c = 0.592746$ [45].

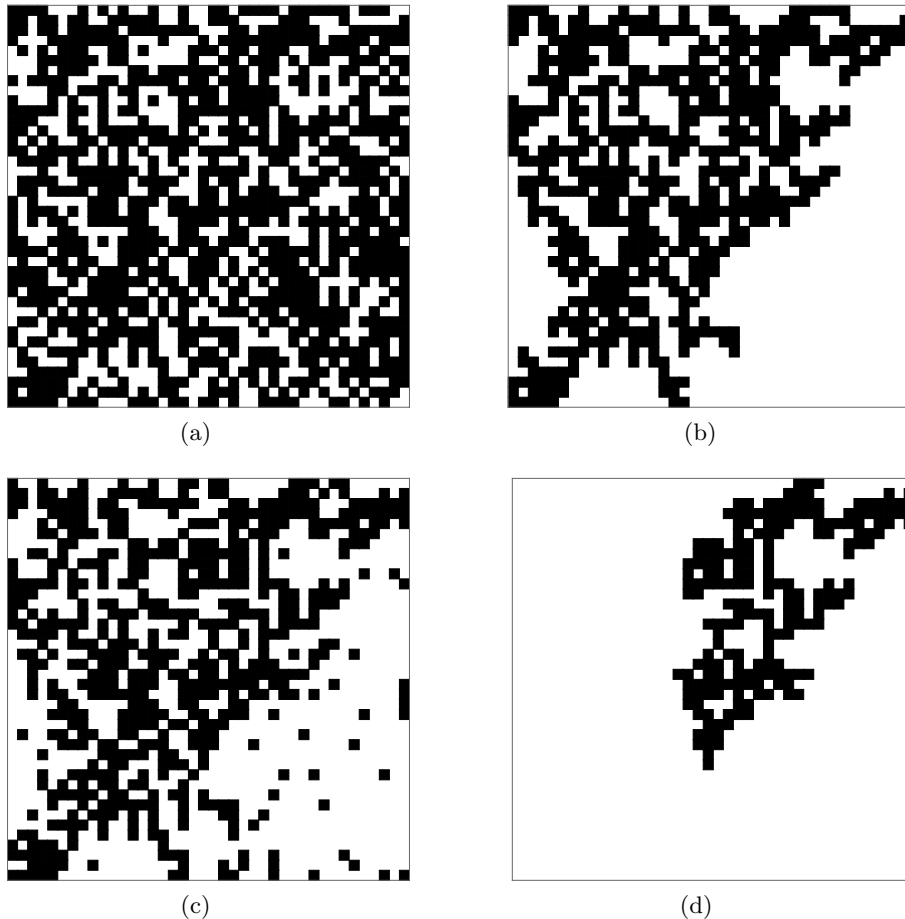


FIG. 1. In this article, we examine four distinct configurations that we have studied. **a** is the raw configuration. **b** is the maxtree of raw configuration. **c** shows the shuffled form of **b** with a ratio $r = 0.2$. **d** shows the maxtree of fig **c**.

B. Methods

1. PCA

PCA [28] stands as a statistical technique that operates by taking a collection of measurements, potentially interrelated, and transforming them into a fresh ensemble of measurements devoid of intercorrelation. These novel measurements are termed principal components. The transformation is meticulously devised to ensure that the initial principal component encapsulates the maximum variability within the data, with each successive component capturing as much variability as feasible while maintaining independence from its predecessors.

A primary application of PCA lies in diminishing the data's dimensionality while conserving maximal variability. This proves advantageous for data visu-

alization, feature reduction, or preparing the data for subsequent machine learning algorithms. PCA entails the computation of the eigenvalues and eigenvectors of the data's covariance matrix. The eigenvectors, denoted as principal components, delineate the orientations of the new feature space, while the eigenvalues signify their magnitude or the variance along those orientations. Subsequent to extracting the principal components, the data can be projected onto them to effectuate dimensionality reduction.

The process of PCA involves several key steps to reduce the dimensionality of data while preserving its essential information. Initially, the data undergoes preprocessing, where it is standardized to have a mean of 0 and a standard deviation of 1, ensuring uniformity for analysis. Subsequently, the covariance matrix is computed to capture the variance and interactions between variables, offering insights into

their relationships. Following this, eigenvalues and eigenvectors are calculated to define new axes for the data, where eigenvalues signify the variance explained by each eigenvector and eigenvectors dictate the principal component directions. These eigenvalues and eigenvectors are then sorted to determine the most significant components, aiding in dimensionality reduction. From this sorted list, a subset is selected based on the desired number of dimensions for the reduced data, focusing on principal components that contribute most to the variance. Finally, the original data is projected onto the selected eigenvectors, effectively reducing its dimensions while retaining as much pertinent information as possible. Through these sequential steps, PCA simplifies data representation, facilitating clearer insights into underlying patterns and relationships.

2. AE

An AE epitomizes a specialized iteration of artificial neural networks extensively harnessed within the realm of unsupervised learning endeavors. Its cardinal objective pivots around the meticulous crafting of condensed data representations, intricately mirroring the innate structure of the original dataset. This mission is twofold in nature: first, to curtail the dimensionality of data, and second, to assuage any prevailing noise. AE's ubiquity transcends diverse domains, embracing tasks such as anomaly detection, image denoising, and feature reduction.

The conventional blueprint of an AE is delineated by two pivotal constituents: the encoder and the decoder. The encoder assumes the mantle of compressing input data into a succinct, fixed-size representation christened as the latent-space representation. Conversely, the decoder embarks on the endeavor of reconstructing the input data from the latent-space representation, with the overarching aspiration of engendering an output that faithfully mirrors the original input.

The Mathematical Formulation of encoder can be represented as

$$f(x) = s(Wx + b) \quad (1)$$

The decoder as

$$g(y) = s(Qy + a) \quad (2)$$

where W and Q are weights, b and a are biases, s is an activation function, x is the input, and $y = f(x)$ is the encoded data. The training involves minimizing a loss function $L(x, g(f(x)))$, which measures the

difference between the input x and the reconstructed output $g(f(x))$.

Fully connected Autoencoders (FCAEs) stand as a specialized variant of AE meticulously tailored to efficaciously handle image data, exhibiting enhanced stability compared to Convolutional AE counterparts. These FCAEs harness hidden layers to capitalize on the spatial intricacies inherent in images, thereby preserving pixel relationships. Consequently, FCAEs emerge as adept contenders for a spectrum of image-centric tasks, including but not limited to image denoising, inpainting, and feature learning.

Amidst the encode-decode process, hidden layers pivot towards local feature extraction, leveraging weight sharing to curtail the plethora of trainable parameters. Subsequently in Back propagation, gradient descent algorithm come into play to Renewal Neuron weight parameter, thus the accuracy of calculation is guaranteed. Activation functions, notably Rectified Linear Unit (ReLU), find ubiquitous application post each Neurons, infusing non-linearity into the network's fabric. In the decoder realm, upsampling layers are enlisted to reinstate image dimensions to their original magnitudes. Minimization loss function assumes primacy, serving as a quintessential metric for assessing the network's adeptness in reconstructing the input image.

III. THE UNSUPERVISED LEARNING RESULTS

In the traditional Ising model, the order parameter manifests as the average magnetization strength. Within the context of the two-dimensional lattice model of the Ising model, this parameter is derived by computing the average of all spin magnetic moments. However, the order parameter of the site percolation model diverges from this paradigm, necessitating the computation of the probability that an individual site pertains to the percolation cluster to ascertain its representation. Given the close association between the critical value of the site percolation model and the percolating cluster, our study endeavors to scrutinize the interplay between clusters within the site percolation model and latent variables in unsupervised learning.

Typically, PCA's first principal component and AE's single latent variable are deemed instrumental in extracting the critical values of the phase transition model. To elucidate this relationship comprehensively, we endeavor to characterize the raw configuration of site percolation. In this study, we

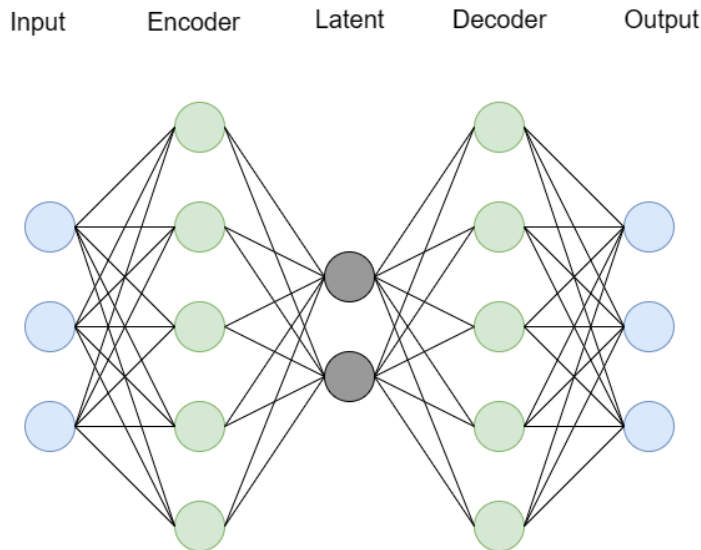


FIG. 2. Neural network schematic structure of autoencoder.

explore four configurations, namely the raw configuration, the maximum cluster, the shuffled maximum cluster, and the maximum cluster after shuffling, as illustrated in Fig. 1. To facilitate a comparative analysis of the results' accuracy, we initially conducted a MC simulation of the raw configuration, wherein the function with the maximum value of the derivative is regarded as the critical point of the model. It's worth noting that the results presented in this paper are normalized for consistency.

As depicted in Fig. 3(a), we conducted simulations on a lattice of size $L = 100$, generated using 1000 probabilities ranging between 0 and 1. For each probability value, we generated the lattice 1000 times and tallied the instances of percolation. The y-axis values were obtained by dividing this count by 1000, while the x-axis represents the generation probability. Notably, Fig. 3(a) exhibits a discernible discontinuity in the curve, indicative of a pronounced peak around 0.59, coinciding closely with our anticipated theoretical value of 0.593. This outcome attests to the efficacy of our simulation methodology and serves as a crucial benchmark for the subsequent analyses presented in this paper.

On the other hand, our investigation also extends to exploring the correlation between particle number density and the critical point in the site percolation model, where the particle number density denotes the ratio of occupied sites to the total lattice sites. Employing this approach, we computed the relationship between particle number density and percola-

tion probability in the site percolation model, as illustrated in Fig. 3(b). Analogous to the preceding method, we simulated a square lattice with dimensions $L = 100$, generating 1000 instances at varying probabilities. Subsequently, we tallied the number of configurations featuring the maximum cluster in each case, serving as a proxy for particle density. The average of these values constitutes the y-axis of Fig. 3(b), while the x-axis represents the generation probability. Notably, Fig. 3(b) reveals a conspicuous peak in the curve, aligning closely with the critical point at approximately 0.59.

A. The raw configurations

As an initial benchmark, we employed the MC to simulate a lattice with a size of $L = 40$ and analyzed the raw configurations. The results, depicted in Fig. 4(a), reveal a linear increase in particle density as the generation probability escalates. In the normalized outcome, particle densities from various sizes exhibit overlapping behavior. However, the outcome lacks discernible non-trivial features and fails to pinpoint the critical points.

Subsequently, we utilized PCA to process the raw configuration of the model, yielding the outcomes of the first principal component, as illustrated in Fig. 4(b). Notably, the results mirror the pattern observed with the MC method, manifesting as an inclined straight line.

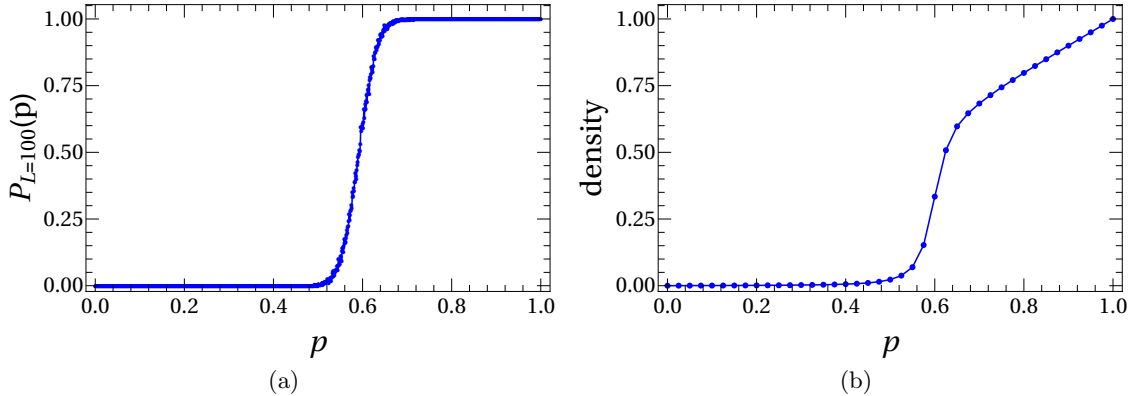


FIG. 3. The MC simulation results about site percolation of a two-dimensional system of size $L \times L$. (a) means the probability that a site belongs to a percolating cluster, (b) calculated the particle number density of the system.

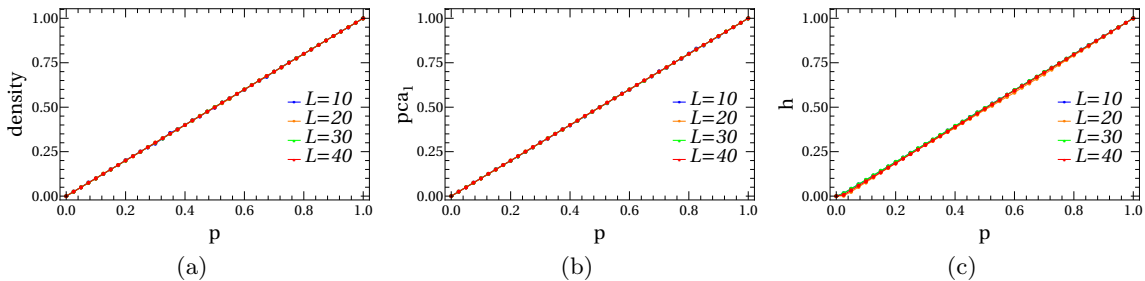


FIG. 4. The experimental results of the raw configurations are shown in the following figures: Figure **a** displays the results of Monte Carlo simulation, Figure **b** shows the results of PCA, and Figure **c** demonstrates the results of AE.

Finally, we fed the same data into the AE network and obtained the distribution of the single latent variable h at different scales, as depicted in Fig. 4(c). Remarkably, akin to the preceding cases, the distribution function exhibits a robust linear relationship. As the model generation probability escalates, h demonstrates a monotonic increase. However, this approach fails to facilitate the identification of the critical point of the system.

Drawing from our understanding of the site percolation model, an augmentation in the generation probability invariably culminates in a linear escalation of the model's particle density, corroborated by the findings of the MC simulation. Nevertheless, what piques our interest is that both PCA and AE manifest some form of linear relationship. This prompts us to speculate whether the input of the model's configuration information into PCA and AE yields a relationship between the first principal component of PCA (pca_1) and the single hidden variable (h) with respect to particle density. We intend to undertake a comprehensive verification of this hypothesis in the ensuing chapter.

B. The maximum cluster

In the preceding discussion, we extensively examined the experimental results pertaining to the raw configurations in MC, PCA, and AE. Now, let's delve into the configurations associated with the order parameter in the percolation model, specifically focusing on the maximum cluster configuration. As previously mentioned, the occurrence of phase transition in this model predominantly manifests within the largest clusters. To commence, we shall scrutinize the MC results obtained from a lattice with dimensions $L = 40$, depicted in Figure 5(a). In contrast to the experimental outcomes of the original configurations, the function curve in this instance exhibits curvature. Notably, from Figure 5(a), we can discern the position of the maximum value of the function's derivative, which corresponds to the inflection point, or the critical point. This point is situated in close proximity to the theoretical critical value of $p_c = 0.593$.

Confronted with the non-linear curve depicted in

intersection size \ size	L_{10}	L_{20}	L_{30}	L_{40}
L_{20}	P_{10-20}			
L_{30}		P_{20-30}		
L_{40}			P_{30-40}	
L_{50}				P_{40-50}

TABLE I. This table presents the critical values of the two-dimensional site percolation model ($L = 40$) under three different methods, MC, PCA, and autoencoder, where the shuffle ratio of the maximum cluster is $r = 0.2$.

Fig. 5(a), we encounter challenges in fitting these data points efficiently. To quantitatively derive a reasonable threshold value, we propose a method akin to Finite Size Scaling (FSS), provisionally termed as Fake Finite Size Scaling (FFSS). The methodology is as follows: Initially, we generate particle density versus percolation probability plots for five different site percolation sizes corresponding to $L = 10, 20, 30, 40, 50$, with an ensemble number of 500. Subsequently, utilizing Mathematica software, we identify the intersections of $L = 10$ and $L = 20$ as (L_{10-20}, P_{10-20}) . By extension, we derive four intersection points, as delineated in Tab. I. Through extrapolation to these intersections with FFSS, we approximate the critical value $p_c = 0.595(2)$ as the system approaches infinity in Figure 5(d). Remarkably, this result aligns with theoretical predictions. Although this approach diverges from the standard finite-size scaling methodology, it holds merit to a certain extent.

Simultaneously, PCA and AE were leveraged to analyze the maximum cluster, yielding the results depicted in Fig. 5(b) and (c) respectively. In Fig. 5(b), employing the PCA method, we observe a function form akin to that in Fig. 5(a), for which we encounter challenges in identifying an optimal fitting method. Consequently, we resort to employing the FFSS method proposed earlier to ascertain the critical point within the PCA framework. The FFSS corresponding to Fig. 5(b) is illustrated in Fig. 5(e), yielding an extrapolated value in the thermodynamic limit of $p_c = 0.597(4)$, which aligns with theoretical expectations. In contrast, the extraction of a single latent variable (h) using the AE yields the result depicted in Fig. 5(c), where h VS P conforms to a standard sigmoid function. In this scenario, we directly employ Mathematica’s sigmoid function to fit the data, yielding a critical value of $p_c = 0.590(9)$, consistent with the theoretical critical value. The FSS result is showed in Fig. 5(f). Consequently, we posit that both PCA and AE can yield analogous results when analyzing the maximum cluster, effectively capturing the critical point of the site perco-

lation system.

C. The shuffled maximum cluster

Upon scrutinizing the outcomes derived from analyzing both the raw configuration and the maximum cluster, we have delineated two plausible explanations for the observed results. Firstly, it appears that the maximum cluster harbors critical information of significance. Secondly, there exists the possibility that unsupervised learning methodologies are solely capable of calculating the particle density within the configuration. To substantiate these hypotheses, we conducted a shuffling experiment on the maximum cluster. Should we attain similar results as those obtained with the unaltered maximum cluster (depicted in Fig. III B) using randomly shuffled maximum clusters, it would corroborate that the first principal component of PCA and the single latent variable of the AE indeed encapsulate the particle number density. Conversely, disparate outcomes would imply that they represent alternative facets of the system.

Utilizing a random shuffling process with a ratio of 0.2, we perturbed the maximum cluster and employed the altered configuration to conduct experiments utilizing the three aforementioned methods. The results are illustrated in Fig. 6. Upon comparison of Fig. 6(a) with Fig. 5(a), it becomes evident from the MC experiment outcomes that the particle number density remains unaltered. Intriguingly, akin to Fig. 5(b), similar outcomes are observed in Fig. 6(b), with negligible alterations in shape and the critical point persisting around 0.593. Similarly, Fig. 6(c) yields outcomes analogous to those of Fig. 5(c). This preliminary evidence indicates that the PCA and AE methods exclusively provide insights into the particle number density of the system phase.

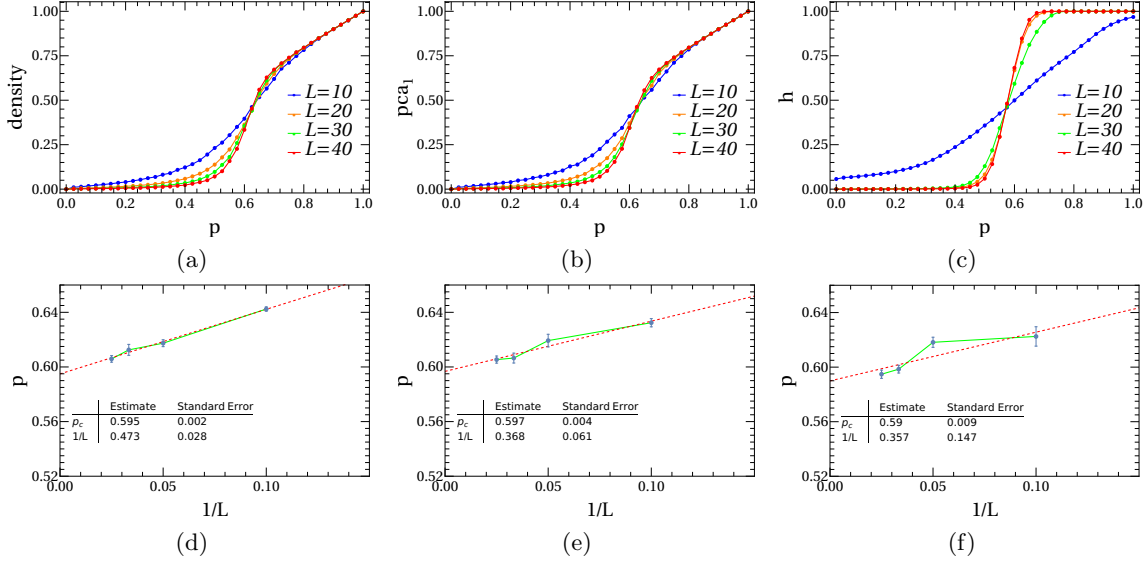


FIG. 5. The results of two-dimensional site percolation with the maximum cluster selected from the raw configuration. The vertical coordinates of Panels **a-c** denote the particle density, the first principal component of PCA, and the single latent variable of AE, respectively. Their horizontal coordinates are all percolation probabilities. Panels **d-f** then correspond to FFSS, FFSS and FSS, respectively.

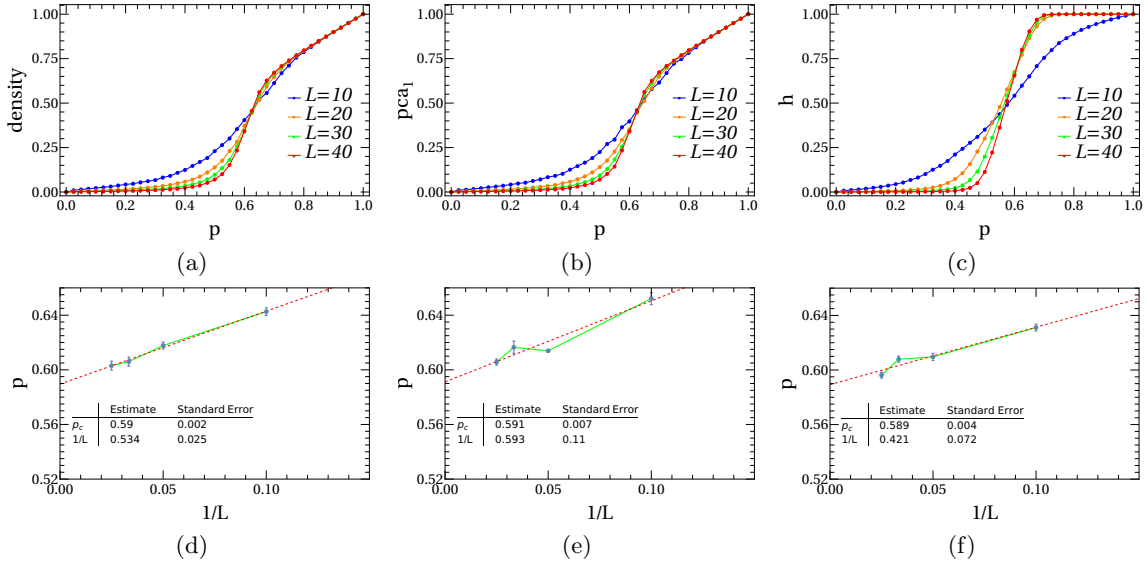


FIG. 6. The results of two-dimensional site percolation with the shuffled maximum cluster. The vertical coordinates of Panels **a-c** denote the particle density, the first principal component of PCA, and the single latent variable of AE, respectively. Their horizontal coordinates are all percolation probabilities. Panels **d-f** then correspond to FFSS, FFSS and FSS, respectively.

D. The maximum cluster of shuffled maximum cluster

Lastly, we extracted the maximum cluster from the shuffled configuration to diminish the number of

particles in the configuration while retaining the information pertaining to the maximum cluster. This serves as a secondary method to validate our hypothesis. If we procure akin learning outcomes as those derived from the unaltered maximum cluster, it in-

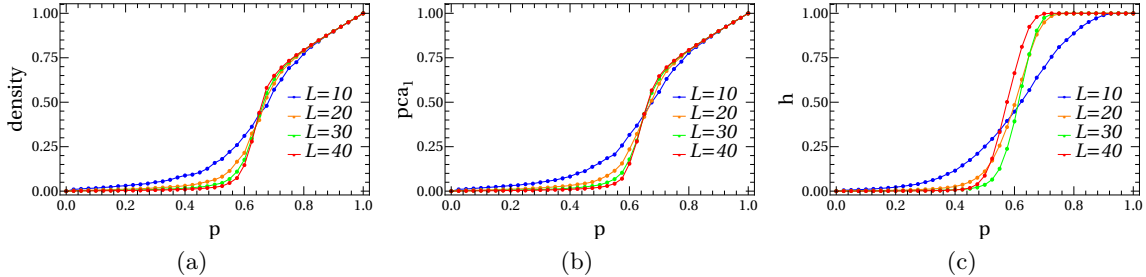


FIG. 7. The experimental results involve selecting the maximum cluster from the shuffled maximum cluster. panel (a) shows the results of the MC simulation, panel (b) the results of PCA, and panel (c) the results of AE.

indicates that ML can discern certain order parameter information from the maximum cluster. Conversely, disparate learning outcomes would imply that the results obtained through ML are inherently linked to particle density information.

The results of the MC simulation are depicted in Fig. 7(a). At this juncture, we have significantly altered the original configuration by first extracting the maximum cluster and subsequently shuffling it with a certain ratio. Consequently, the spatial correlation of the system has undergone modification. Thus, discussing the phase transition points of the system may no longer be appropriate. However, to encapsulate the overall alteration in this configuration, we opted to employ the term "jumping location". As evidenced by Fig. 7(a), the jumping location appears to shift towards the right. This phenomenon can be attributed to the reduction in particle number density of the extracted maximum cluster following the shuffled configuration.

Fig. 7(b) showcases the outcome of the first principal component of PCA. Notably, the jumping location of the curve also shifts towards the right, mirroring the trend observed in the MC results. The remarkable concurrence between the MC particle number density outcomes and the first principal component of PCA lends credence to the notion that the primary information encapsulated by the first principal component of PCA pertains to the particle number density. This observation underscores that PCA predominantly captures the density of particles, rather than the specific arrangement of particles. Once again, it is demonstrated that PCA learns the particle number density rather than the order parameter.

To further substantiate this perspective, we conducted learning experiments using an AE neural network. Fig. 7(c) illustrates the learning outcome of the AE's single latent variable. Notably, the jumping location depicted in Fig. 7(c) does not exhibit

a pronounced shift towards the right. This discrepancy could potentially be attributed to the small shuffle ratio ($r = 0.2$).

In order to delve into the impact of the shuffle ratio on the jumping location in greater detail, we maintained the system size at $L = 40$ and shuffled the maximum cluster at varying ratios, namely 0, 0.2, 0.4, 0.6, 0.8, and 1. These modified configurations were then fed into PCA and autoencoder for learning, respectively, as depicted in Fig. 8. Fig. 8(a) displays the PCA results, wherein a discernible rightward shift in the jumping location of the curve is evident with increasing shuffling ratio when the system size remains constant. Similarly, Fig. 8(b) presents the results obtained from the AE. Analogous to PCA, an unmistakable rightward shift in the jumping location of the function is observed as the shuffling ratio escalates. This further underscores that both methods primarily capture the particle number density of the configuration rather than the order parameter. For more detailed AE results, refer to Tab. II. The jumping location in Tab. II is determined through sigmoid function fitting. It is evident that as the shuffling ratio increases, the jumping location also increases, underscoring the robustness of the AE's single latent variable results.

E. Discussions

The four parts above respectively explore four different configurations of site percolation using MC simulations and unsupervised learning techniques: the raw configuration, the maximum cluster, the shuffled maximum cluster, and the maximum cluster after shuffling. These findings are summarized in Tab. III. The raw configuration of site percolation is randomly generated, and the particle number density does not reveal critical information, thus no critical point is identified in this column. In the

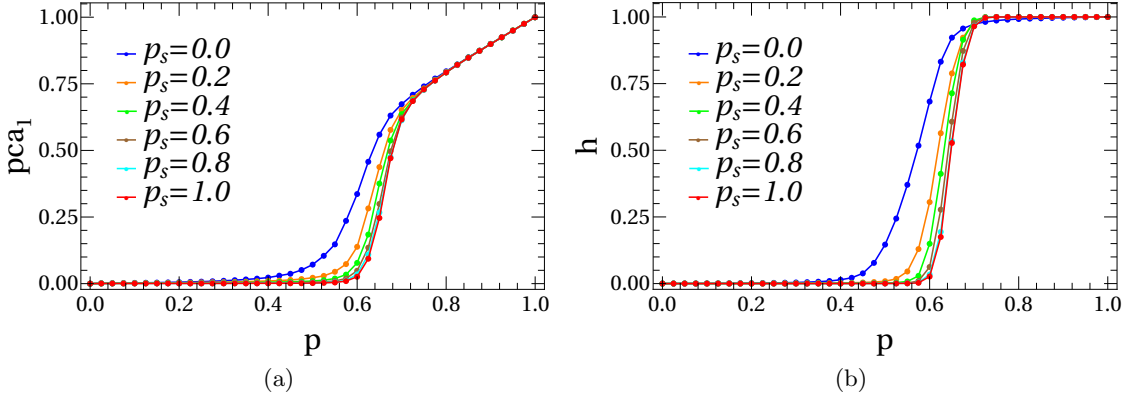


FIG. 8. The experimental results of selecting the maximum cluster from the raw configuration and shuffling it to select the maximum cluster conformations are obtained. The system size is fixed at $L = 40$, and different shuffling ratios are used for the learning results. Panel **a** shows the results of PCA, and panel **b** shows the results of AE.

r (shuffle ratio)	0	0.1	0.2	0.3	0.4	0.5	0.6	0.7	0.8	0.9	1.0
jumping location	0.5695(6)	0.6020(4)	0.6192(2)	0.6274(2)	0.6323(2)	0.6384(2)	0.6423(2)	0.6454(1)	0.6482(2)	0.6491(2)	0.6491(2)

TABLE II. AE results of two-dimensional site percolation with different shuffle ratios, where $L = 40$. The second row in the table represents the single potential variable results of the maximum cluster after shuffling the maximum cluster with different shuffle ratios.

method	configuration		
	raw	maximum cluster	shuffled maximum cluster
MC(<i>density</i>)	None	0.595(2)	0.590(2)
PCA(<i>pca</i> ₁)	None	0.597(4)	0.591(7)
AE(<i>latent</i>)	None	0.590(9)	0.589(4)

TABLE III. This table presents the critical values of the two-dimensional site percolation model ($L = 40$) under three different methods, MC, PCA, and AE, where the shuffle ratio of the maximum cluster is $r = 0.2$.

maximum cluster column of Tab. III, we employ three methods to ascertain the critical value. The results indicate that the maximum cluster can effectively represent the critical information of the site percolation model. This observation motivates further investigation into the relationship between particle number density, PCA's first principal component, autoencoder's individual latent variables, and order parameters.

In the shuffled maximum cluster column of Tab. III, all three methods still capture the critical point of the model effectively. This suggests that PCA's first principal component and autoencoder's single latent variable precisely extract the number of particles in the system, which appears to have little association with the specific spatial arrangement of the particles. Lastly, a similar study is conducted

on the maximum cluster after shuffling. Due to the altered spatial correlation of the system, discussion shifts from the system's phase transition point to the jumping location, illustrating the influence of shuffle ratio.

IV. CONCLUSION

The primary objective of this study was to investigate the particle density and critical point of site percolation using finite size scaling. Through thorough examination of various configurations of the model, we posited that the single latent variable of the AE and the first principal component of PCA may not represent the order parameter of the model, but rather could potentially reflect the particle den-

sity.

To test this hypothesis regarding particle density, we conducted a randomized shuffling of the maximum clusters of the percolation model. Subsequently, we extracted PCA's first principal component and AE's single latent variable based on the shuffled configurations. Through unsupervised learning on both the raw and shuffled configurations of the maximum clusters, we confirmed that PCA's first principal component and AE's single latent variable can effectively represent the particle density of site percolation.

Nevertheless, shuffling the system impacts the size of the maximum cluster. Upon analyzing the remaining maximum cluster after applying different shuffling ratios, we observed that this manipulation alters the correlation within the percolation model, consequently inducing a certain degree of shift in the critical point position of the system.

The findings indicate a robust correlation between PCA's first principal component and AE's single latent variable with the particle density of the percolation model. This study lays the groundwork for investigating percolation systems, enabling the effective extraction of critical points and physical

quantities dependent on particle density through unsupervised learning. Notably, PCA's first principal component and AE's single latent variable precisely capture the number of particles in the system, rather than the order parameter. This insight can offer valuable guidance for ML approaches applied to percolation-like phase transitions, including percolation-like Ising models.

V. ACKNOWLEDGEMENTS

This work was supported in part by Key Laboratory of Quark and Lepton Physics (MOE), Central China Normal University (Grant No. QLPL2022P01), Research Fund of Baoshan University (BYPY202216, BYKY202305), Wen Bangchun Academician Workstation (202205AF150032), the Fundamental Research Funds for the Central Universities, China (Grant No. CCNU19QN029), the National Natural Science Foundation of China (Grant No. 61873104), the 111 Project, with Grant No. BP0820038.

-
- [1] M. I. Jordan and T. M. Mitchell, *Science* **349**, 255 (2015).
 - [2] I. Goodfellow, Y. Bengio, and A. Courville, *Deep learning* **1**, 98 (2016).
 - [3] B. Mahesh, *International Journal of Science and Research (IJSR)* **Volume 9 Issue 1** (2020).
 - [4] A. Engel and C. Van den Broeck, *Statistical mechanics of learning* (Cambridge University Press, 2001).
 - [5] P. Mehta, M. Bukov, C.-H. Wang, A. G. Day, C. Richardson, C. K. Fisher, and D. J. Schwab, *Physics reports* **810**, 1 (2019).
 - [6] G. Carleo, I. Cirac, K. Cranmer, L. Daudet, M. Schuld, N. Tishby, L. Vogt-Maranto, and L. Zdeborová, *Reviews of Modern Physics* **91**, 045002 (2019).
 - [7] J. Carrasquilla, *Advances in Physics: X* **5**, 1797528 (2020).
 - [8] H. Ajakan, P. Germain, H. Larochelle, F. Laviolette, and M. Marchand, arXiv preprint arXiv:1412.4446 (2014).
 - [9] J. Hammersley, *Monte carlo methods* (Springer Science & Business Media, 2013).
 - [10] C. Domb, *The critical point: a historical introduction to the modern theory of critical phenomena* (CRC Press, 1996).
 - [11] H. Hinrichsen, *Advances in physics* **49**, 815 (2000).
 - [12] D. J. Amit and V. Martin-Mayor, *Field Theory, the Renormalization Group, and Critical Phenomena: Graphs to Computers Third Edition* (World Scientific Publishing Company, 2005).
 - [13] J. Carrasquilla and R. G. Melko, *Nature Physics* **13**, 431 (2017).
 - [14] W. Zhang, J. Liu, and T.-C. Wei, *Physical Review E* **99**, 032142 (2019).
 - [15] E. P. Van Nieuwenburg, Y.-H. Liu, and S. D. Huber, *Nature Physics* **13**, 435 (2017).
 - [16] L. Wang, *Physical Review B* **94**, 195105 (2016).
 - [17] J. Shen, W. Li, S. Deng, and T. Zhang, *Physical Review E* **103**, 052140 (2021).
 - [18] J. Shen, F. Liu, S. Chen, D. Xu, X. Chen, S. Deng, W. Li, G. Papp, and C. Yang, *Physical Review E* **105**, 064139 (2022).
 - [19] J. Shen, W. Li, S. Deng, D. Xu, S. Chen, and F. Liu, *Scientific Reports* **12**, 19728 (2022).
 - [20] S. J. Wetzel, *Physical Review E* **96**, 022140 (2017).
 - [21] C. Wang and H. Zhai, *Physical Review B* **96**, 144432 (2017).
 - [22] W. Hu, R. R. Singh, and R. T. Scalettar, *Physical Review E* **95**, 062122 (2017).
 - [23] P. Zhang, C. Moore, and L. Zdeborová, *Physical Review E* **90**, 052802 (2014).
 - [24] J. Wang, W. Zhang, T. Hua, and T.-C. Wei, *Physical Review Research* **3**, 013074 (2021).

- [25] K. Pearson, The London, Edinburgh, and Dublin Philosophical Magazine and Journal of Science **2**, 559 (1901).
- [26] Y. Ganin, E. Ustinova, H. Ajakan, P. Germain, H. Larochelle, F. Laviolette, M. Marchand, and V. Lempitsky, The journal of machine learning research **17**, 2096 (2016).
- [27] Eaton.Eric and R. Mansbach, in *Proceedings of the AAAI Conference on Artificial Intelligence*, Vol. 26 (AAAI Press, Palo Alto, California, 2012) pp. 900–906.
- [28] H. Abdi and L. J. Williams, Wiley interdisciplinary reviews: computational statistics **2**, 433 (2010).
- [29] L. Van der Maaten and G. Hinton, Journal of machine learning research **9** (2008).
- [30] L. Van Der Maaten, The Journal of Machine Learning Research **15**, 3221 (2014).
- [31] H. Boursard and Y. Kamp, Biological cybernetics **59**, 291 (1988).
- [32] L. Malo Roset, *Applications of machine learning to studies of quantum phase transitions*, Master’s thesis, Universitat Politècnica de Catalunya (2019).
- [33] G. E. Hinton and R. S. Zemel, Advances in neural information processing systems **6**, 3 (1994).
- [34] G. E. Hinton and R. R. Salakhutdinov, science **313**, 504 (2006).
- [35] W. M. Kouw and M. Loog, arXiv preprint arXiv:1812.11806 (2018).
- [36] P. Huembeli, A. Dauphin, and P. Wittek, Physical Review B **97**, 134109 (2018).
- [37] P. Ponte and R. G. Melko, Physical Review B **96**, 205146 (2017).
- [38] S. J. Wetzel and M. Scherzer, Physical Review B **96**, 184410 (2017).
- [39] R. Jadrach, B. Lindquist, and T. Truskett, The Journal of chemical physics **149**, 194109 (2018).
- [40] S. Jianmin, W. Shanshan, L. Wei, X. Dian, Y. Yuxiang, W. Yanyang, G. Feng, Z. Yueying, and T. Kui, arXiv preprint arXiv:2311.11741 (2023).
- [41] W. Xu, J. He, and Y. Shu, Advances and Applications in Deep Learning , 45 (2020).
- [42] K. Ch’Ng, J. Carrasquilla, R. G. Melko, and E. Khatami, Physical Review X **7**, 031038 (2017).
- [43] J. W. Essam, Reports on progress in physics **43**, 833 (1980).
- [44] F. D’Angelo and L. Böttcher, Phys. Rev. Research **2**, 023266 (2020).
- [45] K. Christensen and N. R. Moloney, *Complexity and criticality*, Vol. 1 (World Scientific Publishing Company, 2005).